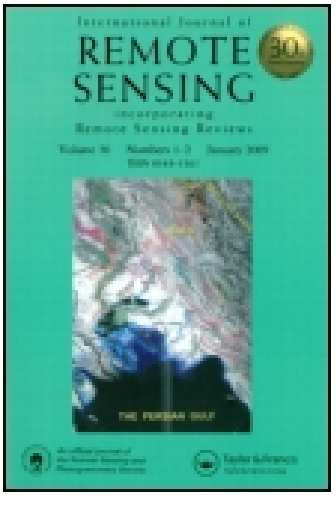

International Journal of Remote Sensing

Publication details, including instructions for authors and subscription information:
http://www.tandfonline.com/loi/tres20

DEM-based modification of pixel-swapping algorithm for enhancing floodplain inundation mapping

Chang Huang[ab], Yun Chen[b] & Jianping Wu[a]

[a] Key Laboratory of Geographic Information Science, Ministry of Education, East China Normal University, Shanghai 200241, China

[b] Land and Water, CSIRO, Canberra 2601, Australia

Published online: 20 Dec 2013.

To cite this article: Chang Huang, Yun Chen & Jianping Wu (2014) DEM-based modification of pixel-swapping algorithm for enhancing floodplain inundation mapping, International Journal of Remote Sensing, 35:1, 365-381, DOI: 10.1080/01431161.2013.871084

To link to this article: http://dx.doi.org/10.1080/01431161.2013.871084

International Journal of Remote Sensing, 2014
Vol. 35, No. 1, 365–381, http://dx.doi.org/10.1080/01431161.2013.871084

Taylor & Francis
Taylor & Francis Group

DEM-based modification of pixel-swapping algorithm for enhancing floodplain inundation mapping

Chang Huang[a,b]*, Yun Chen[b], and Jianping Wu[a]

[a]*Key Laboratory of Geographic Information Science, Ministry of Education, East China Normal University, Shanghai 200241, China;* [b]*Land and Water, CSIRO, Canberra 2601, Australia*

(*Received 22 June 2013; accepted 27 October 2013*)

Floodplain inundation plays a key role in riparian ecosystems. Remote sensing provides an advanced technology for detecting floodplain inundation, but the trade-off between the spatial and temporal resolutions of remotely sensed imagery is a well-known issue. Sub-pixel mapping is an effective way to mitigate the trade-off by improving the spatial resolution of image classification results while keeping their temporal resolution. It is therefore useful for improving the mapping of highly dynamic flood inundation using coarse-resolution images. However, traditional sub-pixel mapping algorithms have limitations on delineating the extent of floodplain inundation that reveals linear and complex characteristics. A modified pixel-swapping (DMPS) algorithm which is based on a digital elevation model (DEM) is thus developed in this study. It is built on the widely accepted pixel-swapping (PS) algorithm and one of its derivatives, the linearized pixel-swapping (LPS) algorithm. A Landsat image recording a significant flood inundation event in the Chowilla Floodplain of the Murray–Darling Basin in Australia was used as a case study. The results show that the DMPS algorithm outperformed the original PS and LPS algorithms both in accuracy and rationality of the resultant map. It improves the accuracy and the kappa coefficient by about 5% and 0.1, respectively, in comparison with the PS algorithm. The spatial pattern of inundation derived from the DMPS algorithm reveals fewer breakpoints and errors along the river channels. Moreover, it is observed that the DMPS algorithm is less sensitive to some critical parameters compared with the PS and LPS algorithms. It is hoped that the proposed DMPS algorithm will broaden the application of coarse-resolution sensors in floodplain inundation detection, which would thereby benefit the ecological studies in floodplains.

Keywords: sub-pixel mapping; super-resolution mapping; lidar DEM; remote sensing; inundation detection

1. Introduction

River floodplains are very important to humanity and the environment. They not only serve as buffers against the effects of extreme floods and droughts, but also support riparian ecosystems, both in quantity and diversity (Arnesen et al. 2013). The spatial and temporal pattern of flood inundation is critical to the distribution of flora and fauna (Townsend and Walsh 1998; Ordoyne and Friedl 2008). Inundation mapping, therefore, plays a crucial role in the ecological studies of floodplains. Remotely sensed imagery has been widely used in inundation detection (Brivio et al. 2002; Di Baldassarre, Schumann, and Bates 2009; Auynirundronkool et al. 2012; Huang, Chen, and Wu 2014) because of

*Corresponding author. Email: chang.huang@outlook.com

its efficiency on continuously acquiring ground information at various scales. Numerous sensors have been proved to be able to map inundation (Islam and Sado 2000; Toyra, Pietroniro, and Martz 2001; Schumann, Di Baldassarre, and Bates 2009; Islam, Bala, and Haque 2010; Chen et al. 2011, 2012, 2013), but none of them are suitable for all situations (Osorio and Galiano 2012; Huang, Chen, and Wu 2013). Medium- to high-resolution images, such as Landsat Thematic Mapper/Enhanced Thematic Mapper Plus (TM/ETM+) and Advanced Land Observation Satellite (ALOS), are typically available fortnightly or less often, which limits their application for intensively and continuously monitoring flood events. Whereas coarse-resolution sensors such as the Advanced Very High Resolution Radiometer (AVHRR) or Moderate Resolution Imaging Spectroradiometer (MODIS) scan the earth's surface once or several times a day, they have coarse spatial resolution, which hampers the correct mapping of flooded areas. There is often a trade-off between the temporal and spatial resolutions of remotely sensed imagery.

Super-resolution mapping, also known as sub-pixel mapping, is a method that aims to mitigate this trade-off by increasing the spatial resolution of soft classification results from remotely sensed images (Atkinson 2005). In contrast to hard classification, which assigns one class to each individual pixel, soft classification derives a fraction map for each class. The fraction map only maintains the proportion of the same class within each pixel, without specifying the location of the class. Many algorithms have been developed to spatially allocate sub-pixels within each coarse pixel of fraction maps, such as the Hopfield Neural Network (Tatem et al. 2002), genetic algorithm (Mertens et al. 2003), pixel attraction models (Mertens et al. 2006; Ling et al. 2010; Ling et al. 2013), and pixel-swapping (PS) algorithm (Atkinson 2005; Thornton, Atkinson, and Holland 2006, 2007; Makido, Shortridge, and Messina 2007; Shen, Qi, and Wang 2009; Su et al. 2012). Although these algorithms use different approaches, their foundation is similar. They are all based on the spatial correlation of land cover information, referring to the tendency for spatially proximate observations of a land cover feature to be more alike than more distant observations (Tatem et al. 2001; Atkinson 2005). Focusing on maximizing the spatial correlation between neighbouring sub-pixels without integrating information on the direction of variation, these methods tend to produce convex shapes which represent most ground features. However, they are generally inappropriate for mapping linear features such as roads and rivers. As floodplain inundation starts from the overbank flow of rivers, inundation extent always reveals linear characteristics. Conventional sub-pixel mapping algorithms are thus unsuitable for floodplain inundation detection.

Thornton et al. (2007) developed a linearised PS (LPS) algorithm for mapping rural linear land cover features from fine-resolution remotely sensed imagery. An anisotropic distance-decay model was employed to replace the isotropic model in the conventional PS algorithm. The direction used in the anisotropic model was estimated by examining the largest neighbouring proportions to enhance the prediction of linear features. However, this might cause misleading direction information when mapping inundation, especially at the meanders and confluences of rivers, which makes the LPS algorithm imperfect for flood inundation mapping at a sub-pixel scale.

It is believed that when additional information on class distribution patterns is available at a sub-pixel level, more accurate sub-pixel mapping can be achieved (Nguyen, Atkinson, and Lewis 2005, 2006). Because floodplain inundation extent has a close relationship with topography, digital elevation models (DEMs) at sub-pixel-level resolutions are considered to be valuable in providing supplementary information (Nguyen, Atkinson, and Lewis 2005; Ling et al. 2008). A common method of inundation sub-pixel mapping using DEM data is to assign flooded sub-pixels directly based on the elevation

(Ling et al. 2008; Osorio and Galiano 2012; Li et al. 2013). However, this method usually produces many gaps, speckles, and irregular shapes in the primary results, and requires complicated post-clean-up processing. Moreover, the accuracy of this method relies highly on the accuracy of DEM data. For radar-derived DEM data, errors are frequently produced because of the common radar speckles. These errors may cause problems for sub-pixel mapping using this method. Except for elevation, DEM data can be used to derive a wealth of information about the morphology of the land surface, such as slope, aspect, flow direction, and flow accumulation (Jenson and Domingue 1988). Streams can also be derived from DEM data, which provides a spatial network with important direction information that is useful for improving sub-pixel mapping of floodplain inundation extent. Therefore, streams, rather than elevation data, were used for supporting sub-pixel mapping in this study, which lowers the dependence on DEM data, in terms of DEM data accuracy. The iterative optimization method of PS the algorithm was employed to avoid the post-processing of the existing method.

This study, therefore, aims to achieve an improved accuracy for efficiently mapping inundation extent using coarse-resolution images at a sub-pixel scale. The objectives are (1) to develop a modified sub-pixel mapping algorithm based on conventional PS and LPS algorithms by employing a finer-resolution DEM; (2) to optimize parameters in the modified algorithm; and (3) to evaluate the accuracy of the modified algorithm in mapping floodplain inundation using a case study.

2. Methods

A new sub-pixel mapping method called the DEM-based modified PS (DMPS) algorithm was developed in this study. It introduced DEM data into the conventional PS and LPS algorithms. Modifications were made mainly in two procedures, the initialization of the sub-pixel map and the distance-decay model for attractiveness calculation. The summary flowchart of the three algorithms is sketched in Figure 1. Detailed descriptions are presented in the following sections.

2.1. PS algorithm and LPS algorithm

The PS is an algorithm initially proposed by Atkinson (2005) to achieve the maximum attractiveness between same-class fractions. The input to PS is the fraction map which maintains the class proportion within each coarse pixel. For each pixel, a fixed number of sub-pixels is created based on a predefined scale factor (S). The scale factor refers to the scale ratio between the coarse pixel and the sub-pixel. For example, if $S = 5$, then 25 sub-pixels will be created in each coarse pixel. The PS algorithm begins with an initialization which allocates sub-pixels randomly within the coarse pixel according to the proportion of the target class. Then the attractiveness of all sub-pixels is calculated based on their initial locations. For each sub-pixel i, its attractiveness A_i is calculated as a distance-weighted function of its $j = 1, 2, \ldots, J$ neighbouring sub-pixels:

$$A_i = \sum_{j=1}^{J} \lambda_{ij} C_j, \tag{1}$$

where C_j is the binary class (1 for the target class and 0 for the other) of the jth pixel, and λ_{ij} is a distance-dependent weight predicted using a distance-decay model as:

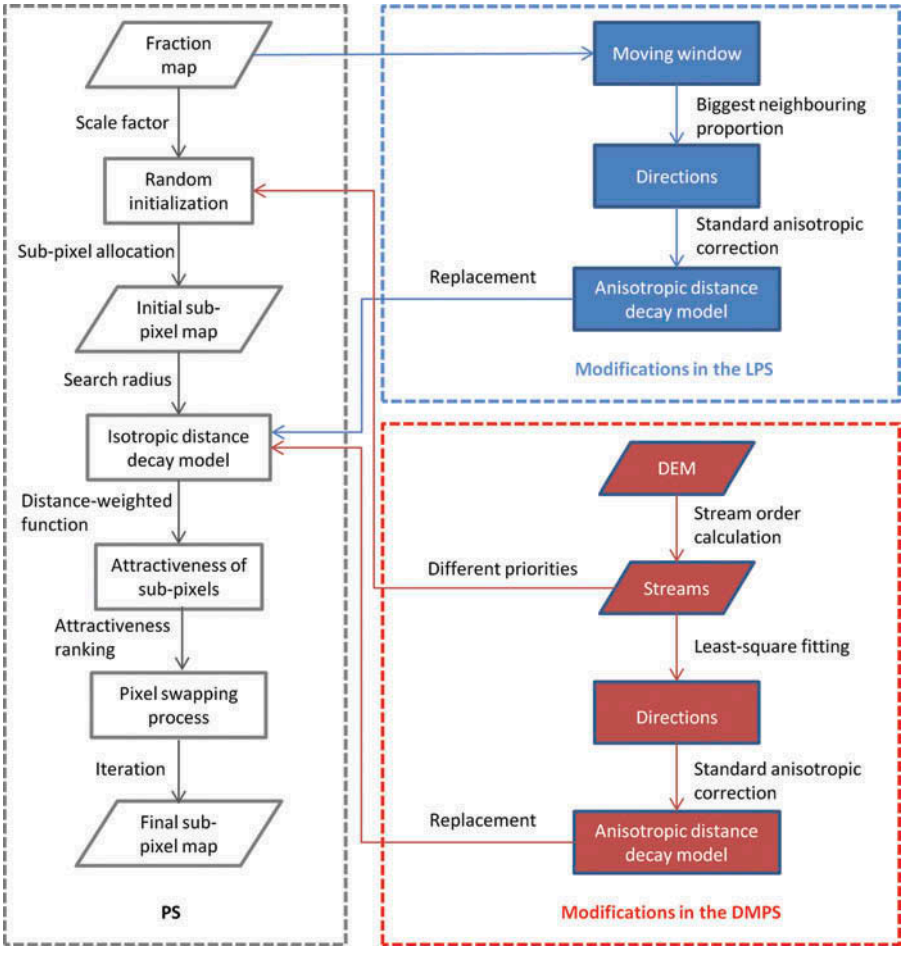

Figure 1. Flowchart of sub-pixel mapping algorithms showing their major procedures. The grey frame shows the basic procedures of the PS algorithm. The blue frame shows the modifications to the PS algorithm in the LPS algorithm. The red frame shows the modifications to the PS algorithm in the DMPS algorithm.

$$\lambda_{ij} = \exp\left(\frac{-h_{i,j}}{\alpha}\right), \tag{2}$$

where α is the exponential parameter of the distance-decay model, and $h_{i,j}$ is the Euclidean distance between the location of sub-pixel i and a neighbouring sub-pixel j. A vector $\boldsymbol{h}$ was introduced as

$$\boldsymbol{h} = \begin{bmatrix} h_x \\ h_y \end{bmatrix} = \begin{bmatrix} x_j - x_i \\ y_j - y_i \end{bmatrix}. \tag{3}$$

$h_{i,j}$ then equals the modulus of vector $\boldsymbol{h}$ (Equation (4)). The Euclidean distance is isotropic, which means the PS algorithm uses an isotropic distance-decay model:

$$h_{i,j} = \|\boldsymbol{h}\| = \sqrt{h_x^2 + h_y^2}. \tag{4}$$

The total number of neighbouring sub-pixels (J) is determined by a value of radius (r) that is used to search neighbours (i.e. neighbour radius). J is calculated as:

$$J = (2r+1)^2 - 1. \tag{5}$$

The algorithm then ranks the attractiveness of sub-pixels on a pixel-by-pixel basis within each coarse pixel. Finally, sub-pixel classes are swapped if the attractiveness at the least attractive location of class 1 is less than that at the most attractive location of class 0. Otherwise, no change will be made. The related attractiveness is updated whenever a change is made. The pixel-swapping process is repeated iteratively until a solution is achieved. It stops either at a fixed number of iterations or when the algorithm converges to a solution.

The PS algorithm was further developed by Thornton et al. (2007) as the LPS algorithm to increase the likelihood of mapping linear features. In contrast with the isotropic distance-decay model in the PS, the LPS employs a unique anisotropic distance-decay model in each coarse pixel, on the basis of estimated directions from the class proportions. In a 3 × 3 moving window applied to the class proportions on the fraction map, with the centre coarse pixel P as the target, the suggested direction inside pixel P is extracted as the straight line connecting the two coarse pixels with largest proportions (Figure 2(*a*)). The direction estimated within the moving window is employed to modify the distance-decay model using the standard anisotropic correction (Goovaerts 1997). The shape of the modified model changes from ellipsoid to circular, with an anisotropy ratio (η) defining the ratio between the minor range and the major range of the ellipse. The coordinate of vector $\boldsymbol{h}$ is transformed as

$$\boldsymbol{h}' = \begin{bmatrix} h'_\phi \\ h'_\psi \end{bmatrix} = \begin{bmatrix} 1 & 0 \\ 0 & \eta \end{bmatrix} \begin{bmatrix} h_\phi \\ h_\psi \end{bmatrix} = \begin{bmatrix} 1 & 0 \\ 0 & \eta \end{bmatrix} \begin{bmatrix} \cos\theta & -\sin\theta \\ \sin\theta & \cos\theta \end{bmatrix} \begin{bmatrix} h_x \\ h_y \end{bmatrix}, \tag{6}$$

where η is the anisotropy ratio and θ is determined by the estimated direction. The anisotropic distance between sub-pixels i and j is then calculated as the modulus of

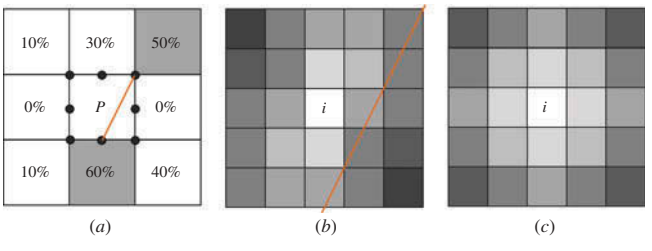

Figure 2. (*a*) Example class proportions extracted from a fraction map in a 3 × 3 moving window for estimating the direction of pixel P. In this example, a direction shown as the line is predicted, as decided by the shaded neighbours; (*b*) anisotropic distance-decay model for sub-pixel i inside pixel P (S = 5) with a direction indicated by the line. Darker colour denotes lower weight; (*c*) isotropic distance-decay model for sub-pixel i inside pixel P (S = 5). Darker colour denotes lower weight.

vector $\boldsymbol{h'}$. Figure 2(*b*) shows the anisotropic distance-decay model within the target pixel P when $S = 5$ in comparison to the isotropic distance-decay model shown in Figure 2(*c*).

In some cases, when there are more than two neighbours that have the same largest proportion in the moving window, a pair of pixels that have a largest distance will be selected, i.e. a pair of diagonal pixels is preferred. There is also a probability that directions cannot be detected for the target pixel in a moving window when all the neighbours have the same proportion. Under this circumstance, the standard isotropic distance-decay model will be used for calculating attractiveness of the sub-pixels inside the target pixel.

Directions estimated from the moving window are reliable only when the shapes of linear features are simple. For flood-inundated areas where river tributaries are dense and river channels are meandering, misleading direction information is often derived. The estimated directions using a moving window can hardly represent the complex flood water dynamic properly, which therefore makes the LPS inappropriate for floodplain inundation mapping at sub-pixel scale.

2.2. *DEM-based modified PS (DMPS) algorithm for inundation mapping*

To overcome the drawbacks in the PS and LPS methods, DEM data at sub-scale resolution were introduced to modify these algorithms. With topographic information provided by the DEM, the movement of surface water can be predicted, in forms of flow direction and flow accumulation. Streams along with stream order can be derived from the flow direction and flow accumulation raster. Stream order raster assigns a numeric order to links in a stream network in order to identify and classify types of streams based on their numbers of tributaries (Tarboton, Bras, and Rodriguez-Iturbe 1991). There are two commonly used methods to assign orders. One is the Shreve method (Shreve 1966), where orders are additive downslope; whenever two streams intersect, their orders are added and assigned to the downslope stream. The other is the Strahler method (Strahler 1957), which increases the order only when streams of the same order intersect. The Strahler method is relatively better for the modification of the algorithm because the main stream is easier to trace using the Strahler order. And the main stream is able to provide valuable information on the pattern of floodplain inundation extent.

The DMPS uses the stream order raster derived from the DEM data as additional input data. For each coarse pixel with a scale factor of S, there are $S \times S$ related stream order pixels calculated from the DEM (Figure 3(*a*)). Within each coarse pixel, main stream pixels were identified by taking those pixels with the highest stream order value (Figure 3 (*b*)). Two major modifications were then made based on the PS and LPS algorithms using the identified main stream pixels.

The first modification is the initial allocation of sub-pixels. Different from the random initialization in the PS and the LPS algorithm, sub-pixels at the locations of main stream pixels were assigned as inundated pixels with the highest priority in the DMPS algorithm. These sub-pixels were given a special and higher value (C_j) rather than 1 in order to secure the importance of main streams in floodplain inundation. $(1 + r)$ was found to be an appropriate value, where r is the neighbour radius (see as Equation (5)). After the main stream pixels were assigned, other locations with higher stream order values had higher priorities to be assigned as water. Figure 3(*c*) shows the initial assignment of a water proportion of 40% within the coarse pixel (i.e. 10 sub-pixels need to be assigned as inundated) along high stream order pixels. After locations with a stream order of 10 and 5

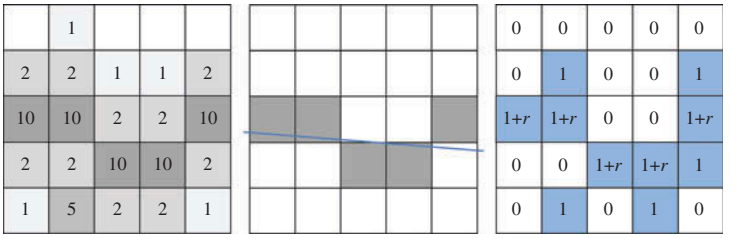

Figure 3. (*a*) Stream order values at sub-pixel scale within a coarse pixel (scale factor $S = 5$); (*b*) main stream pixels (shown as shaded) identified by selecting those with the highest stream order value. The direction shown by the line was estimated by linear least-square fitting these main stream pixels. $R^2 = 0.08$; (*c*) initial allocation of a 40% inundation proportion within a 5 × 5 sub-pixel window. Main stream pixels were assigned a special and higher value ($1 + r$), where r is the neighbour radius. Locations with higher stream order values were assigned as inundated with higher priorities. Blue pixels were allocated as inundated.

were assigned, four sub-pixels were selected randomly from locations with a stream order of 2 to be assigned as inundated (Figure 3(*a*)).

The second modification is the distance-decay model used for attractiveness calculation. Main stream pixels were employed to estimate directions that can help improve the anisotropic distance-decay model in the LPS algorithm. A linear least-square fitting was applied using the main stream pixels to derive a line which predicts the direction information (Figure 3(*b*)). The goodness-of-fit of the linear regression is usually evaluated using the coefficient of determination (R^2; $0 \le R^2 \le 1$). However, it is generally believed that an arbitrary benchmark of R^2 is not suitable for judging the fitness (Barrett 1974). In this case, main stream pixels were identified within an $S \times S$ grid space. It was found that even when the fitted line was considered acceptable for representing the distribution of main stream pixels, the R^2 could sometimes be very small (as in Figure 3(*b*)). Therefore, the fitted line was adopted as the estimated direction in this study regardless of its R^2 value. It has to be noted that under certain circumstance, there might be no main stream pixel identified within a coarse pixel, for example in plain areas where all stream order values are NULL. Then the moving window approach (as shown in Figure 2) would be employed to derive direction. The estimated direction was then applied to the anisotropic distance-decay model to calculate the distance-dependent weight for the attractiveness of sub-pixels.

3. Case study

3.1. Data preparation

A case study area located at the Chowilla Floodplain of the Murray–Darling Basin (MDB) of Australia (Figure 4(*a*)) was selected. It covers about 181,360 ha, including a large water body (Lake Victoria), a section of the main channel of the Murray River, and its tributaries.

The inundation map (Figure 4(*b*)), which comprised 1700 × 1120 pixels, was derived from a Landsat ETM+ image at 30 m resolution using the modified normalized difference water index (mNDWI; (Xu 2006)). The Landsat image was acquired on 13 December 2000, when there was a significant flood event in the study area. The mNDWI is one of the most popular indices for inundation detection (Huang et al. 2012). It was calculated using a combination of reflectances in the Green band (Band 2 of Landsat TM/ETM+

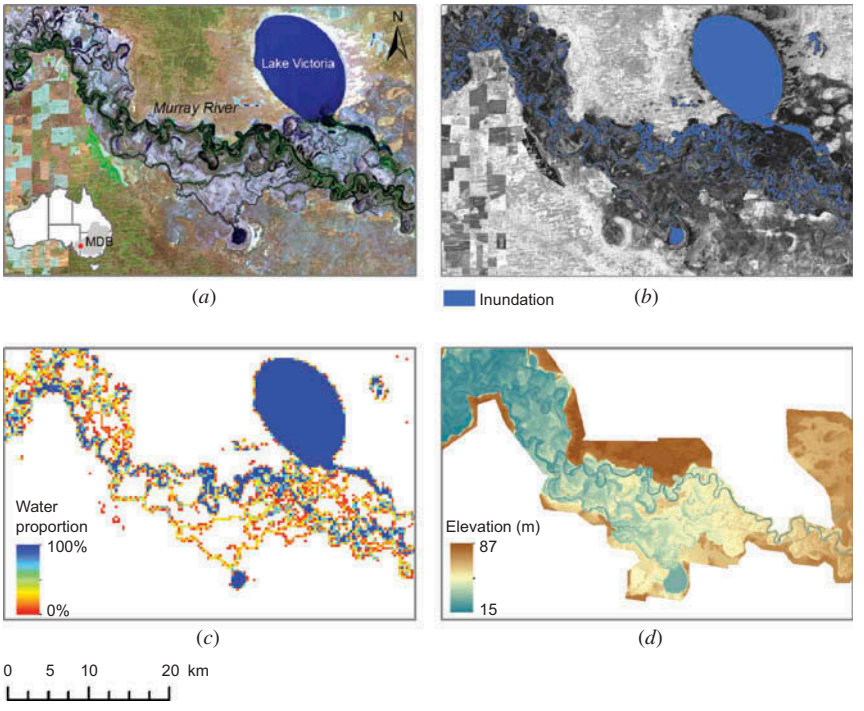

Figure 4. Materials of case study. (*a*) Major water bodies and location of study area shown in a colour composite (R2G4B7) Landsat ETM+ image; (*b*) original inundation map derived from the Landsat ETM+ mNDWI image at a resolution of 30 m; (*c*) water fraction map maintaining water proportion of each 300 m coarse pixel. It was derived by aggregating the original inundation map with a scale factor of 10, and was used as the input of sub-pixel mapping; (*d*) 5 m DEM data applied to the DMPS algorithm for inundation mapping.

image) and Short-Wave Infrared (SWIR) band (Band 5 of Landsat TM/ETM+ image) as Equation (7). The inundation map (Figure 4(*b*)) was used to generate the fraction map as the input to sub-pixel mapping. It was also used as the reference image for accuracy evaluation:

$$\mathrm{mNDWI} = (\mathrm{Green} - \mathrm{SWIR})/(\mathrm{Green} + \mathrm{SWIR}). \quad (7)$$

The basic input of sub-pixel mapping is a fraction map, which is commonly derived from image soft classification. In this study, a degraded fraction map was used in order to avoid errors and uncertainties introduced by image soft classification. The degradation procedure was to aggregate pixels from the Landsat-derived inundation map in a window of size according to the required scale factor (S) into a coarse pixel. The proportion of the coarse pixel was calculated by dividing the number of inundated pixels by the window size. In this case, S was set to 10. The original inundation map (Figure 4(*b*)) was aggregated by a 10×10 window with the aggregated pixel value equalling the proportion of inundated pixels inside this window (Figure 4(*c*)). The resolution of the aggregated fraction map will thus be 300 m.

Airborne light detection and ranging (lidar) provides an effective way for acquiring three-dimensional terrain point data with high density and high accuracy. One of the

appealing features in lidar products is the lidar DEM. Lidar DEM data at 5 m resolution (Figure 4(*d*)) were employed to provide additional information at the subscale for the DMPS algorithm. The DEM data were resampled to 30 m using the bilinear interpolation method in order to match the sub-pixel size. Sinks that existed in the DEM were filled using the ArcGIS Hydrology tool. Flow direction and flow accumulation were then derived. After that, a stream order image was generated based on flow direction and flow accumulation using the Strahler method in the ArcGIS environment. It was then used as an additional input to the DMPS algorithm.

3.2. *Parameter optimization*

In order to evaluate the modified algorithm by comparison with conventional algorithms, all three algorithms (PS, LPS, and DMPS) were employed to derive inundation maps at sub-pixel scale from the input fraction map (Figure 4(*c*)). Several parameters, including neighbour radius (r), exponential parameter of distance-decay function (α), and anisotropy ratio (η) are important to the accuracy of sub-pixel mapping in these algorithms. Therefore, it is necessary to test them with a wide range of parameter values. It was noted that the choice of parameter values is determined by the scale factor S and the input data. With $S = 10$ in this case study, five different values for r and α, and three different η values were tested (see as Table 1). All possible combinations were examined for parameter optimization.

The neighbour radius (r) controls the impact scope of a single sub-pixel. It was initially set to 1 to increase the speed of the algorithm, but small r often causes local convergence. Nevertheless, it has been found that r should be less than S to ensure a given sub-pixel cannot be attracted by other sub-pixels that belong to a non-neighbouring coarse pixel (Atkinson 2005). The impact of different r values on the resultant map was analysed by using fixed values for the other two parameters (Figure 5). In order to highlight the differences on these maps, only a small region of the entire study area is displayed to demonstrate the mapping results of different parameter values. A colour composite Landsat image, inundation reference image, and DEM data were also displayed for referencing. It can be seen from Figure 5 that a value of 1 is apparently too small for r in all three algorithms. Results are relatively stable for all algorithms when r is equal to or greater than 3.

The exponential parameter of distance-decay model (α) is a parameter that balances the weights of different distances on attractiveness. According to Equation (2), a higher α makes the weight decay slower as distance increases. When α is too small, the weights of the direct-neighbouring pixels are much higher than further neighbours. The effect of this is similar to using a small r. As mentioned above, a small r often causes local convergence, which results in many speckles. When α is too high, the neighbouring pixels within the scope of r can contribute almost evenly to the attractiveness. The inundated sub-pixels will be highly compacted towards the larger inundation extent nearby. Some on the outer ring will be left disconnected because of the restriction of coarse pixels. An appropriate α

Table 1. Values of critical parameters tested in pixel-swapping algorithms.

Parameters	Tested values	Algorithms
Neighbour radius(r)	1, 3, 5, 7, 9	PS, LPS, DMPS
Exponential parameter of distance-decay model (α)	0.50, 1, 2, 5, 10	PS, LPS, DMPS
Anisotropy ratio (η)	0.10, 0.35, 0.50	LPS, DMPS

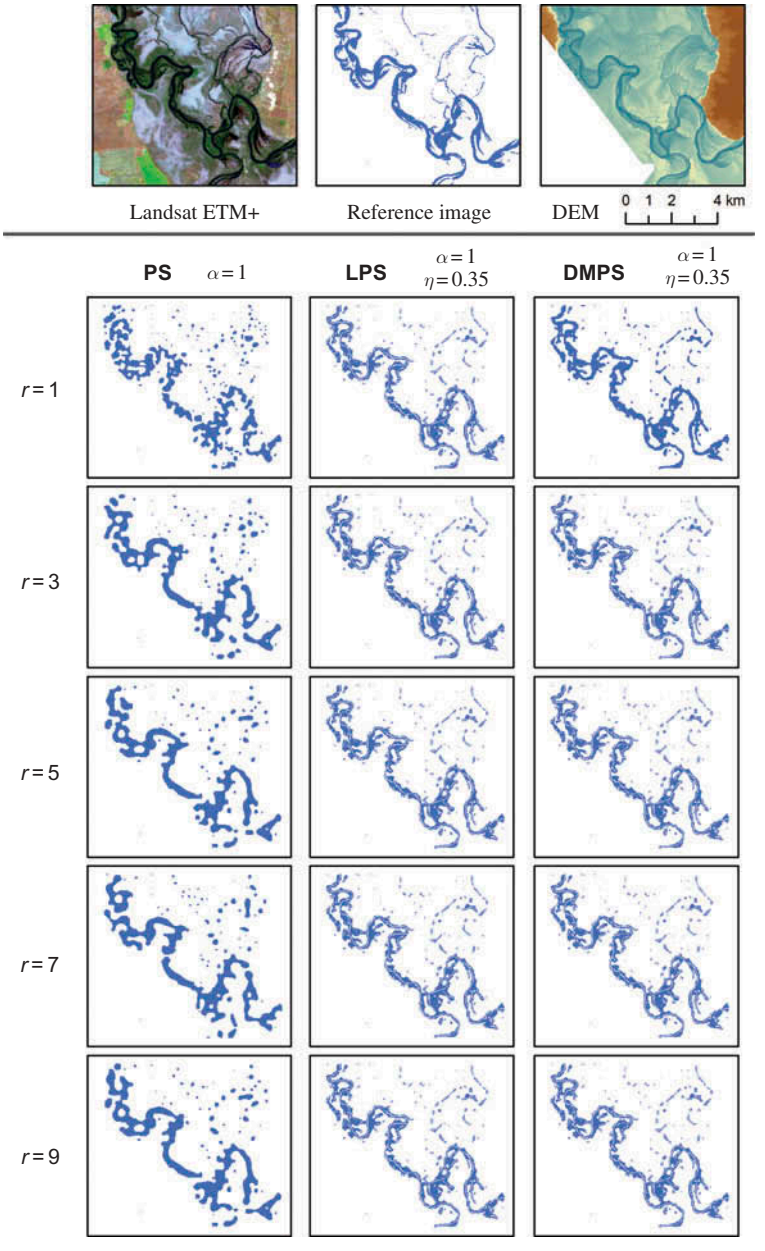

Figure 5. Responses of the three algorithms to different neighbour radius (r) values for the demonstration area, along with colour composite Landsat image, inundation reference image, and DEM data.

will ensure that every sub-pixel within the search radius r contributes significantly and properly to the attractiveness. Figure 6 shows the response of the three algorithms to different α values. Based on the above statement, it was found that a value of 0.5 is too small for α, especially for the PS algorithm, where there are many speckles (especially on the north-eastern corner).

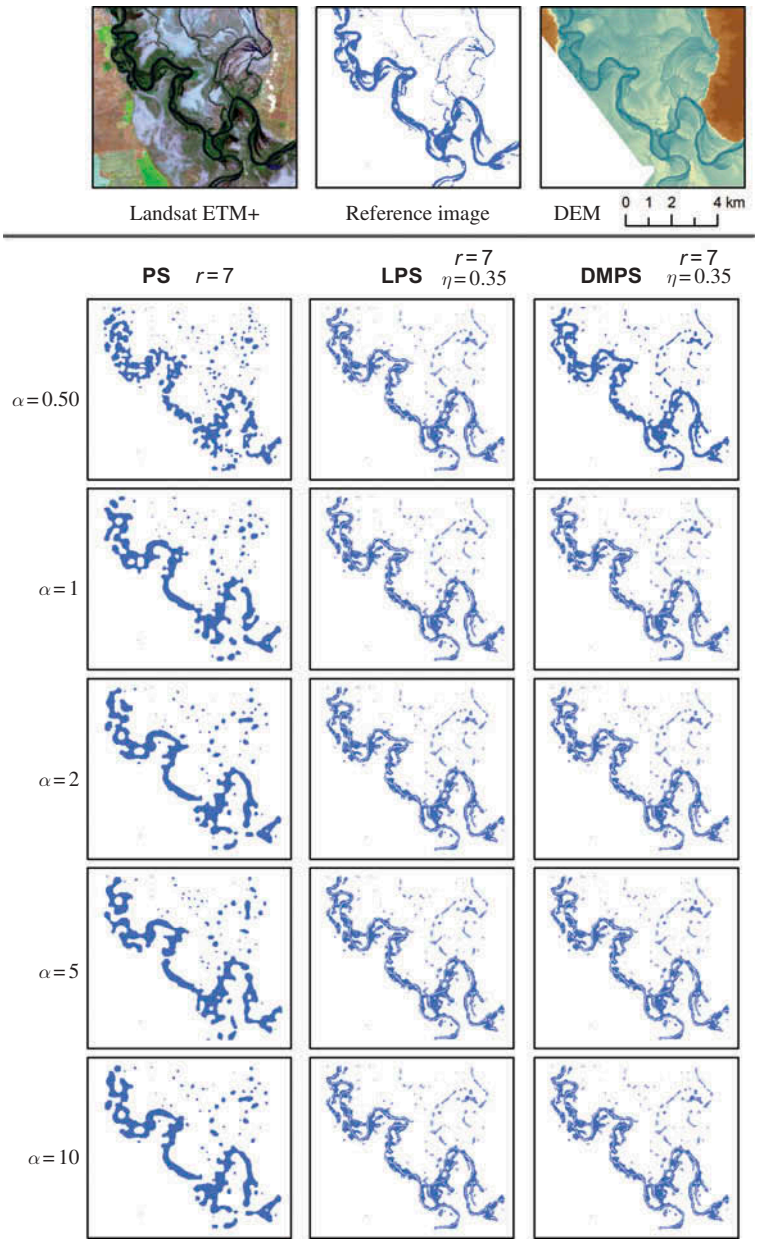

Figure 6. Responses of the three algorithms to different exponential parameter (α) values of the distance-decay model for the demonstration area, along with colour composite Landsat image, inundation reference image, and DEM data.

It was also clear from Figure 6 that a value of 5 or 10 is too big for α, where there are many disconnected linear patches on the out ring of main water bodies. Therefore, a value of 1 or 2 is suggested as a proper choice here. Among these algorithms, LPS and DMPS look to be relatively more stable to different values of α.

Anisotropy ratio (η) is only used when the anisotropic distance-decay model was adopted in calculating spatial attractiveness of sub-pixels. It reveals the contrast of

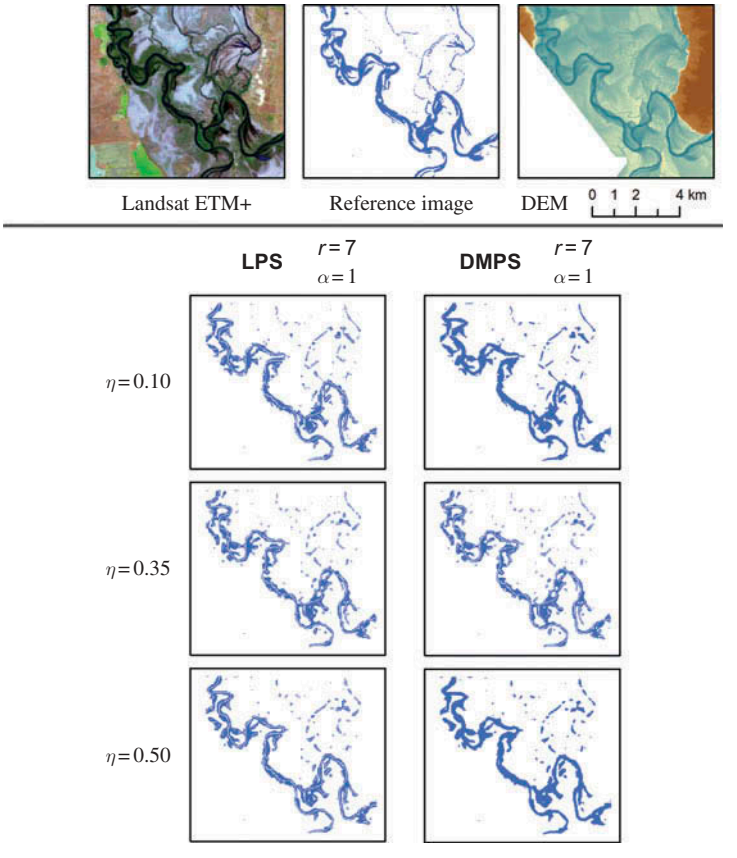

Figure 7. Responses of two algorithms (LPS and DMPS) to different anisotropy ratio (η) values for the demonstration area, along with colour composite Landsat image, inundation reference image, and DEM data.

distance decay between estimated direction and the orthogonal. When η = 1, the LPS algorithm is actually the ordinary PS algorithm. Figure 7 shows the effect of different η values in the LPS and the DMPS algorithms. Smaller η provides sub-pixels on the estimated direction with higher attractiveness, which achieves more significant linear distribution of sub-pixels. However, the trade-off is the decrease of attractiveness on the orthogonal of estimated direction, which may generate gaps and errors. A value of 0.10 was found to be too small for both algorithms. It was also observed that the DMPS is relatively more stable with different η values compared to the LPS.

Based on the above investigation, the resultant maps of this case study using the PS, LPS, and DMPS algorithms with optimal parameter values are shown in Figure 8.

3.3. *Accuracy evaluation*

Accuracy of the resultant maps (Figure 8) derived using the three sub-pixel mapping methods was assessed by comparison with the reference image. Evaluation maps were generated by overlaying the resultant maps and reference image pixel by pixel. Agreement for inundation, commission, and omission errors was identified (Figure 9). Commission

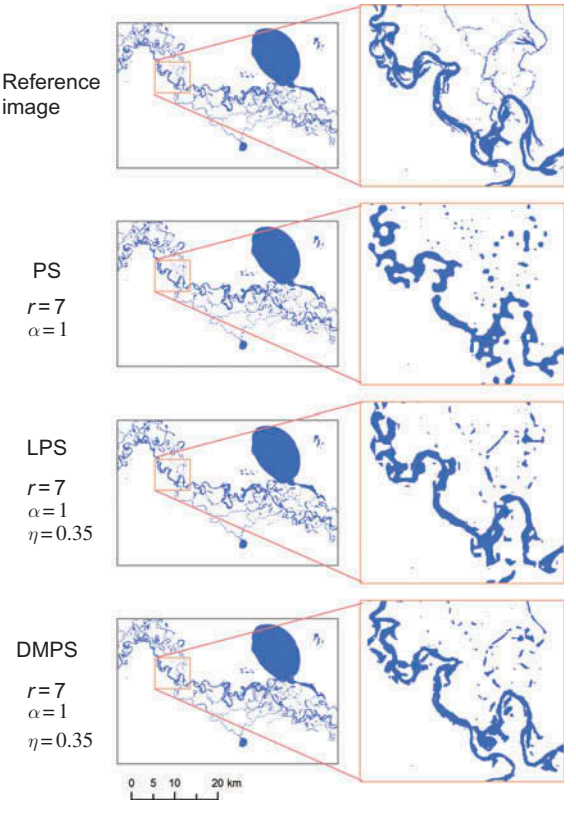

Figure 8. Resultant maps of the PS, LPS, and DMPS algorithms with optimal parameter values, along with the reference image. The left column shows maps of the entire study area; the right column shows maps of the demonstration area.

errors are those pixels that are inundated on the resultant map but not inundated on the reference image. Omission errors are those pixels that are not inundated on the resultant map but inundated on the reference image.

It can be seen from Figure 9 that the large water body (Lake Victoria) was mapped well by all three algorithms. The PS cannot properly map linear features whose width is less than a coarse pixel (Figure 9(*a*)). The inundated pixels in the resultant map tend to gather together, and thus make many discontinuous shapes. Commission and omission errors are widely distributed, not only on the small tributaries, but also on the main channel of the Murray River and other major rivers. The LPS algorithm is better in deriving linear main channel and major rivers (Figure 9(*b*)), but its performance is often unsatisfying when mapping the confluences of multiple linear features. Errors frequently appear at the river meanders and confluences (seen as rectangles in Figure 9(*b*)). Small tributaries can barely be delineated using this algorithm. The DMPS algorithm yields the best sub-pixel inundation map (Figure 9(*c*)). The main channel and major rivers were mapped reasonably well and continuously, and some of the very small tributaries can even be correctly delineated.

Inspired by Mertens et al. (2003), a mask was applied to exclude all pure pixels from the water fraction map when calculating evaluation indices such as the overall accuracy,

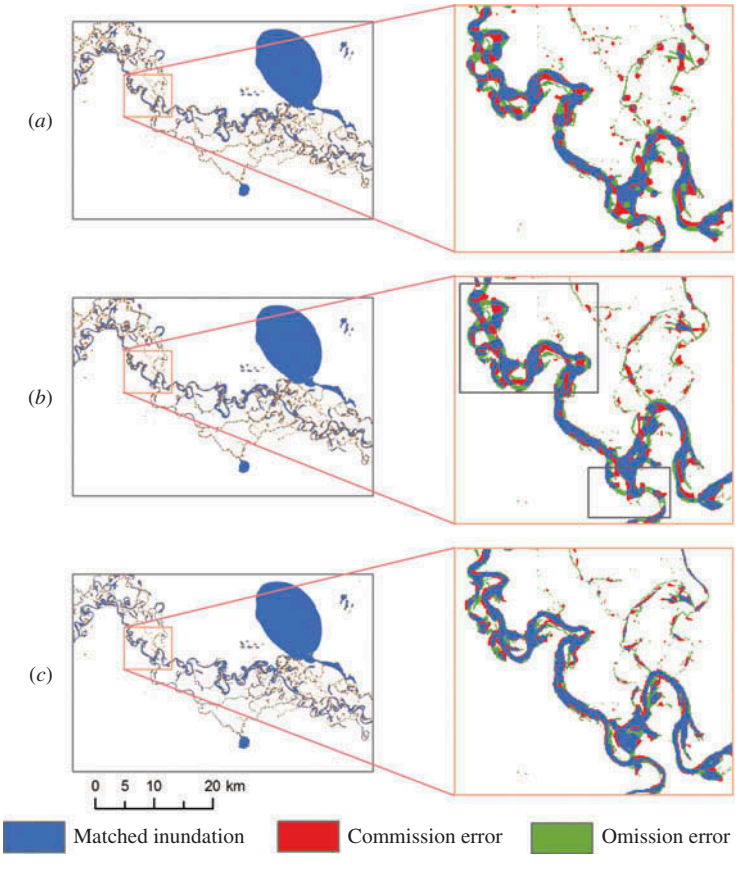

Figure 9. Evaluation maps of different algorithms. The left column shows maps of the entire study area; the right column shows maps of the demonstration area. (*a*) Evaluation map of the original PS algorithm; (*b*) evaluation map of the LPS algorithm; (*c*) evaluation map of the DMPS algorithm.

percentage of commission errors, percentage of omission errors, and kappa coefficient (Table 2). It is quite legitimate to have the same percentage of commission and omission errors here for each algorithm, because the principle of pixel swapping is to swap the locations of sub-pixels that belong to different classes to achieve maximum spatial attractiveness. If there are only two classes, whenever a commission error is produced, there is always a corresponding omission error. The LPS algorithm yields slightly better results than the PS algorithm. The DMPS algorithm produces a better result than both of the other two algorithms: it improves the overall accuracy by about 5% compared with the PS algorithm. This is largely due to the 80% accuracy of the PS algorithm (Table 2), which leaves a maximum improvement space of only 20%. It is believed that the overall accuracy is sometimes subjective (Chen et al. 2013). Therefore, the kappa coefficient is usually introduced to estimate the agreement between two rasters. It is generally thought to be a more robust measurement than overall accuracy because it takes into account the agreement occurring by chance (Chen et al. 2013). As shown in Table 2, the result of the DMPS algorithm has an improved kappa coefficient which is 0.11 and 0.08 higher than the PS and LPS algorithms, respectively. This has demonstrated the merit of the DMPS method. According to Landis and Koch (1977), kappa values from 0.41 to 0.60 and from

Table 2. Indices showing the evaluation results of different algorithms.

Algorithm	Commission error (%)	Omission error (%)	Overall accuracy (%)	Kappa coefficient
PS	10.29	10.29	79.42	0.53
LPS	9.51	9.51	80.98	0.56
DMPS	7.90	7.90	84.20	0.64

0.61 to 0.80 represent moderate agreement and substantial agreement, respectively. A kappa coefficient of 0.64 therefore indicates that the DMPS algorithm is able to derive an inundation map at sub-pixel scale with substantial accuracy, even when applied to complex floodplain inundation conditions.

4. Conclusion

This study further developed the original PS algorithms to incorporate the linear shape information into the super-resolution mapping technology for better detection of river floodplain inundation extent at the sub-pixel scale. Streams derived by DEM were employed to enhance the modified algorithm. Using a case study, the proposed DMPS algorithm was demonstrated to be less sensitive to some critical parameters compared with the PS and LPS methods. It achieves a more accurate super-resolution image, which presents continuous and reasonable river floodplain inundation extent.

Generally speaking, different algorithms suit different situations. For the non-linear sub-pixel mapping issue, the PS algorithm is simple, fast, and efficient. For sub-pixel mapping of simple linear features, applying the LPS algorithm is basically adequate. However, for accurate mapping of floodplain inundation extent to reveal meandering and intersecting linear characteristics, the DMPS algorithm will be a better choice, bearing in mind that the incorporation of DEM data would inevitably increase the run time of the algorithm.

It was also noted that the accuracy of the DEM is vital to the algorithm. As an increasing number of DEM data become available with relatively higher spatial resolutions, such as the Shuttle Radar Topography Mission (SRTM) and lidar, it is hoped that the results of this study will enhance the application of some coarse-resolution images, such as MODIS, in floodplain inundation detection, which would ultimately support the ecological study of floodplains.

Acknowledgements

The authors wish to thank the China Scholarship Council for providing a scholarship to Chang Huang to support this research at CSIRO Land and Water. This work has been conducted under the auspices of the CSIRO Land and Water and Water for a Healthy Country National Research Flagship. The authors are grateful to the NSW Office of Environment and Heritage for providing lidar DEM data for this study. The authors also wish to thank their colleagues Susan Cuddy, Dr Catherine Ticehurst, and Dr Irina Emelyanova for initially reviewing this manuscript. Two anonymous reviewers are acknowledged for their helpful comments.

References

Arnesen, A. S., T. S. F. Silva, L. L. Hess, E. M. L. M. Novo, C. M. Rudorff, B. D. Chapman, and K. C. McDonald. 2013. "Monitoring Flood Extent in the Lower Amazon River Floodplain Using ALOS/PALSAR ScanSAR Images." *Remote Sensing of Environment* 130: 51–61.

Atkinson, P. M. 2005. "Sub-Pixel Target Mapping from Soft-Classified, Remotely Sensed Imagery." *Photogrammetric Engineering and Remote Sensing* 71: 839–846.

Auynirundronkool, K., N. C. Chen, C. H. Peng, C. Yang, J. Y. Gong, and C. Silapathong. 2012. "Flood Detection and Mapping of the Thailand Central Plain Using RADARSAT and MODIS Under a Sensor Web Environment." *International Journal of Applied Earth Observation and Geoinformation* 14: 245–255.

Barrett, J. P. 1974. "The Coefficient of Determination-Some Limitations." *The American Statistician* 28: 19–20.

Brivio, P. A., R. Colombo, M. Maggi, and R. Tomasoni. 2002. "Integration of Remote Sensing Data and GIS for Accurate Mapping of Flooded Areas." *International Journal of Remote Sensing* 23: 429–441.

Chen, Y., S. M. Cuddy, B. Wang, L. E. Merrin, D. Pollock, and N. Sims. 2011. "Linking Inundation Timing and Extent to Ecological Response Models using the Murray-Darling Basin Floodplain Inundation Model (MDB-FIM)." Proceedings of 19th International Congress on Modelling and Simulation (MODSIM2011). Perth, December 12–16.

Chen, Y., C. Huang, C. Ticehurst, L. E. Merrin, and P. Thew. 2013. "An Evaluation of MODIS Daily and 8-Day Composite Products for Floodplain and Wetland Inundation Mapping." *Wetlands* 33: 823–835.

Chen, Y., B. Wang, C. A. Pollino, and L. Merrin. 2012. "Spatial Modelling of Potential Soil Water Retention Under Floodplain Inundation using Remote Sensing and GIS." Proceedings of 2012 International Congress on Environmental Modelling and Software. Leipzig, July 1–5.

Di Baldassarre, G., G. Schumann, and P. Bates 2009. "Near Real Time Satellite Imagery to Support and Verify Timely Flood Modelling." *Hydrological Processes* 23: 799–803.

Goovaerts, P. 1997. *Geostatistics for Natural Resource Evaluation*, 90–95. New York: Oxford University Press.

Huang, C., Y. Chen, and J. Wu. 2013. "A DEM-Based Modified Pixel Swapping Algorithm for Floodplain Inundation Mapping at Subpixel Scale." Proceedings of 2013 IEEE Geoscience and Remote Sensing Symposium (IGARSS2013). Melbourne, July 21–26.

Huang, C., Y. Chen, and J. Wu. 2014. "Mapping Spatio-Temporal Flood Inundation Dynamics at Large River Basin Scale Using Time-Series Flow Data and MODIS Imagery." *International Journal of Applied Earth Observations and Geoinformation* 26: 350–362.

Huang, C., Y. Chen, J. Wu, and J. Yu. 2012. "Detecting Floodplain Inundation Frequency using MODIS Time-Series Imagery." Proceedings of First International Conference on Agro-Geoinformatics (Agro-Geoinformatics 2012). Shanghai, August 2–4.

Islam, A. S., S. K. Bala, and M. A. Haque. 2010. "Flood Inundation Map of Bangladesh Using MODIS Time-Series Images." *Journal of Flood Risk Management* 3: 210–222.

Islam, M. D. M., and K. Sado. 2000. "Development of Flood Hazard Maps of Bangladesh Using NOAA-AVHRR Images with GIS." *Hydrological Sciences Journal-Journal Des Sciences Hydrologiques* 45: 337–355.

Jenson, K., and O. Domingue. 1988. "Extracting Topographic Structure from Digital Elevation Data for Geographic Information System Analysis." *Photogrammetric Engineering and Remote Sensing* 54: 1593–1600.

Landis, J. R., and G. G. Koch. 1977. "The Measurement of Observer Agreement for Categorical Data." *Biometrics* 33: 159–174.

Li, S., D. Sun, M. Goldberg, and A. Stefanidis. 2013. "Derivation of 30-m-Resolution Water Maps from TERRA/MODIS and SRTM." *Remote Sensing of Environment* 134: 417–430.

Ling, F., Y. Du, F. Xiao, H. P. Xue, and S. J. Wu. 2010. "Super-Resolution Land-Cover Mapping Using Multiple Sub-Pixel Shifted Remotely Sensed Images." *International Journal of Remote Sensing* 31: 5023–5040.

Ling, F., X. D. Li, Y. Du, and F. Xiao. 2013. "Sub-Pixel Mapping of Remotely Sensed Imagery with Hybrid Intra- and Inter-Pixel Dependence." *International Journal of Remote Sensing* 34: 341–357.

Ling, F., F. Xiao, Y. Du, H. P. Xue, and X. Y. Ren. 2008. "Waterline Mapping at the Subpixel Scale from Remote Sensing Imagery with High-Resolution Digital Elevation Models." *International Journal of Remote Sensing* 29: 1809–1815.

Makido, Y., A. Shortridge, and J. P. Messina. 2007. "Assessing Alternatives for Modeling the Spatial Distribution of Multiple Land-Cover Classes at Sub-Pixel Scales." *Photogrammetric Engineering and Remote Sensing* 73: 935–943.

Mertens, K. C., B. De Baets, L. P. C. Verbeke, and R. R. De Wulf. 2006. "A Sub-Pixel Mapping Algorithm Based on Sub-Pixel/Pixel Spatial Attraction Models." *International Journal of Remote Sensing* 27: 3293–3310.

Mertens, K. C., L. P. C. Verbeke, E. I. Ducheyne, and R. R. De Wulf. 2003. "Using Genetic Algorithms in Sub-Pixel Mapping." *International Journal of Remote Sensing* 24: 4241–4247.

Nguyen, M. Q., P. M. Atkinson, and H. G. Lewis. 2005. "Superresolution Mapping Using a Hopfield Neural Network with LIDAR Data." *IEEE Geoscience and Remote Sensing Letters* 2: 366–370.

Nguyen, M. Q., P. M. Atkinson, and H. G. Lewis. 2006. "Superresolution Mapping Using a Hopfield Neural Network with Fused Images." *IEEE Transactions on Geoscience and Remote Sensing* 44: 736–749.

Ordoyne, C., and M. A. Friedl. 2008. "Using MODIS Data to Characterize Seasonal Inundation Patterns in the Florida Everglades." *Remote Sensing of Environment* 112: 4107–4119.

Osorio, J. D. G., and S. G. G. Galiano. 2012. "Development of a Sub-Pixel Analysis Method Applied to Dynamic Monitoring of Floods." *International Journal of Remote Sensing* 33: 2277–2295.

Schumann, G., G. Di Baldassarre, and P. D. Bates. 2009. "The Utility of Spaceborne Radar to Render Flood Inundation Maps Based on Multialgorithm Ensembles." *IEEE Transactions on Geoscience and Remote Sensing* 47: 2801–2807.

Shen, Z. Q., J. G. Qi, and K. Wang. 2009. "Modification of Pixel-Swapping Algorithm with Initialization from a Sub-Pixel/Pixel Spatial Attraction Model." *Photogrammetric Engineering and Remote Sensing* 75: 557–567.

Shreve, R. L. 1966. "Statistical Law of Stream Numbers." *Journal of Geology* 74: 17–37.

Strahler, A. N. 1957. "Quantitative Analysis of Watershed Geomorphology." *Transactions American Geophysical Union* 38: 913–920.

Su, Y. F., G. M. Foody, A. M. Muad, and K. S. Cheng. 2012. "Combining Pixel Swapping and Contouring Methods to Enhance Super-Resolution Mapping." *IEEE Journal of Selected Topics in Applied Earth Observations and Remote Sensing* 5: 1428–1437.

Tarboton, D. G., R. L. Bras, and I. Rodriguez-Iturbe. 1991. "On the Extraction of Channel Networks from Digital Elevation Data." *Hydrological Processes* 5: 81–100.

Tatem, A. J., H. G. Lewis, P. M. Atkinson, and M. S. Nixon. 2001. "Super-Resolution Target Identification from Remotely Sensed Images Using a Hopfield Neural Network." *IEEE Transactions on Geoscience and Remote Sensing* 39: 781–796.

Tatem, A. J., H. G. Lewis, P. M. Atkinson, and M. S. Nixon. 2002. "Super-Resolution Land Cover Pattern Prediction Using a Hopfield Neural Network." *Remote Sensing of Environment* 79: 1–14.

Thornton, M. W., P. M. Atkinson, and D. A. Holland. 2006. "Sub-Pixel Mapping of Rural Land Cover Objects from Fine Spatial Resolution Satellite Sensor Imagery Using Super-Resolution Swapping." *International Journal of Remote Sensing* 27: 473–491.

Thornton, M. W., P. M. Atkinson, and D. A. Holland. 2007. "A Linearised Pixel-Swapping Method for Mapping Rural Linear Land Cover Features from Fine Spatial Resolution Remotely Sensed Imagery." *Computers & Geosciences* 33: 1261–1272.

Townsend, P. A., and S. J. Walsh. 1998. "Modeling Floodplain Inundation Using an Integrated GIS with Radar and Optical Remote Sensing." *Geomorphology* 21: 295–312.

Toyra, J., A. Pietroniro, and L. W. Martz. 2001. "Summer Flood Mapping in a Northern Wetland Using a Combination of Radarsat and SPOT Imagery." *Remote Sensing and Hydrology* 2000: 536–538.

Xu, H. Q. 2006. "Modification of Normalised Difference Water Index (NDWI) to Enhance Open Water Features in Remotely Sensed Imagery." *International Journal of Remote Sensing* 27: 3025–3033.